Bull. Mater. Sci. (2022)45:121
https://doi.org/10.1007/s12034-022-02694-5

Z-scheme heterojunction Ag/AgBr/Bi_2MoO_6 with improved visible-light-induced photocatalytic activity

LIFANG CHEN*, LI DING, HONGYE CHENG and ZHIWEN QI
State Key Laboratory of Chemical Engineering, School of Chemical Engineering, East China University of Science and Technology, Shanghai 200237, China
*Author for correspondence (lchen@ecust.edu.cn)

MS received 10 December 2021; accepted 12 February 2022

Abstract. A hierarchical Ag/AgBr/Bi_2MoO_6 heterojunction composite was prepared without the addition of any structure-directing agent via a hydrothermal synthesis combined with subsequent deposition-photoreduction. The obtained samples were characterized by X-ray diffraction, field-emission scanning electron microscopy containing an energy X-ray dispersive spectrometer, X-ray photoelectron spectroscopy, UV–visible diffuse reflectance spectroscopy and photoluminescence spectroscopy. The results demonstrate that the Ag/AgBr/Bi_2MoO_6 composite exhibited enhanced photocatalytic activity under visible-light irradiation for rhodamine B degradation with a rate constant of 0.180 min^{-1}, which was approximately 2.5 times than that of Ag/AgBr and 22.5 times as high as Bi_2MoO_6. In addition, the superior visible light removing efficiencies of methylene blue and colourless phenol further confirmed the broad-spectrum photocatalytic degradation abilities of the Ag/AgBr/Bi_2MoO_6. Moreover, based on band structure analysis and active species trapping experiments, the improved photocatalytic performance of the Ag/AgBr/Bi_2MoO_6 photocatalyst was ascribed to the construction of Z-scheme bridge using Ag nanoparticles, which could increase the separation efficiency of photogenerated electron–hole pairs and keep them with high reduction and oxidation capability.

Keywords. Bi_2MoO_6; Ag/AgBr; Z-scheme; visible light; photocatalysis.

1. Introduction

Toxic organic pollutants in wastewater, as one of the most serious environmental problems, have become an arduous challenge for the sustainable development of modern society [1]. The semiconductor photocatalysts have attracted extensive attention because they can harvest solar energy and eliminate most organic pollutants [2–4]. As known, TiO_2-based photocatalysts are considered attractive due to their low cost and nontoxicity [5]. However, TiO_2 with a large bandgap of 3.2 eV can only absorb less than 5% of solar energy, resulting in very low efficiency of sunlight utilization [6]. Therefore, the development of efficient visible-light responsive photocatalysts has gained great significance. Bismuth-based compounds, such as Bi_2MoO_6 [7], Bi_2WO_6 [8] and $BiVO_4$ [9], as visible-light-active photocatalysts have particularly attracted increasing interest owing to their special electronic configuration and potential catalytic performance.

Bi_2MoO_6 is a layered Aurivillius oxide, consisting of positively charged $[Bi_2O_2]^{2+}$ layers sandwiched between MoO_4^{2-} slabs [7,10]. With a small bandgap of 2.5–2.8 eV, it is capable of capturing visible light and exhibits photocatalytic activity for hydrogen generation from water splitting and organic pollutant degradation [11,12]. However, the improvement of the Bi_2MoO_6 photocatalytic activity is essential because of its poor quantum yield, caused by the rapid recombination of photoinduced charge carriers. To overcome the bottleneck, the coupling of Bi_2MoO_6 with other semiconductors, for example, Bi_2O_3 [13], MoS_2 [14], Bi_2S_3 [15] etc., have been reported to facilitate the separation of photogenerated electron–hole pairs and greatly improve the photocatalytic activity. This may represent a promising and efficient system to enhance visible-light photocatalytic performance, where both semiconductors are photochemical systems that can be excited by visible light. However, the electron transfer in this system is lacking due to the fact that photocatalytic activity depends on not only the electron–hole separation but also interfacial charge transfer. Therefore, it is still a challenge to search for a reasonable strategy to improve the photocatalytic properties of Bi_2MoO_6-based photocatalysts.

Recently, Ag/AgX (X = Cl, Br, I) can be used as cocatalysts to enhance the visible-light photocatalytic activities and stability of semiconductors, e.g., Ag/AgCl/$Bi_2O_2CO_3$ [16], Ag/AgCl/Bi_2MoO_6 [10], Ag/AgBr/BiOBr [17], Ag/AgBr/g-C_3N_4 [18], AgX/Ag_2CrO_4 [19], Ag@AgCl/ZnO [20], Ag@AgBr/$BiPO_4$ [21], Ag/AgBr/$ZnFe_2O_4$ [22], Ag/AgBr/TiO_2 [23], Ag/AgBr/Bi_2MoO_6 [24,25], etc. Thereinto, guest Ag and AgX nanoparticles (NPs) deposited on host

Published online: 30 June 2022

semiconductor materials form a heterojunction structure, where the effective electron–hole pairs separation was photogenerated from guest–host. There are two different roles for the guest Ag NPs due to the photocatalyst and wavelength range of incident light synergistically. When neither guest AgX nor host in the photocatalyst can respond to the incident light, the light absorption of the Ag NPs by the surface plasmon resonance (SPR) is dominant. On the other hand, in a typical Z-scheme Ag/AgBr/BiOBr system [17], where both AgBr and BiOBr can absorb the photons from incident light, the Ag NPs can act as the electron mediator for reducing the distance of Z-scheme electron transfer. As results of the two-step vectorial photoexcitation processes, the composites usually exhibit higher photocatalytic performance than the single-component and binary photocatalysts due to their stronger oxidation and reduction abilities. However, the number of efficient Z-scheme visible-light photocatalysts is still very limited, and the visible-light-active components are mainly restricted to low-band-gap semiconductors. Therefore, the construction of efficient Z-scheme visible-light photocatalysts with visible-light-driven and electron transfer systems is highly desirable.

It is suggested that the Ag/AgBr with SPR effect is beneficial to photocatalytic activity of Ag/AgBr/Bi_2MoO_6 in previous reports [24,25]. A visible-light responsive Ag/AgBr/Bi_2MoO_6 film was prepared by three-step approaches [24]. Another Ag/AgBr/Bi_2MoO_6 was synthesized based on hexadecyltrimethyl ammonium bromide as a structure-directing agent (SDA) to get highly dispersed Ag/AgBr [25]. However, the photocatalytic efficiencies of the Ag/AgBr/Bi_2MoO_6 are not high to satisfy the demand for industrial applications. In this work, we directly construct a Z-scheme system of highly efficient Ag/AgBr/Bi_2MoO_6 composite without the addition of any SDA, where both AgBr and Bi_2MoO_6 can be excited by visible light, while Ag is used as the electron-transfer bridge. This all-solid-state Ag/AgBr/Bi_2MoO_6 photocatalyst with double visible-light-active components exhibited much higher visible-light-driven photocatalytic activity and stability than Bi_2MoO_6, Ag/AgBr, Ag/Bi_2MoO_6 and AgBr/Bi_2MoO_6 for the degradation of nonbiodegradable rhodamine B (RhB), methylene blue (MB) and a colourless phenol. Furthermore, a possible photocatalytic mechanism for the Ag/AgBr/Bi_2MoO_6 composite was proposed to get an insight into the Z-scheme photocatalytic reaction.

2. Materials and methods

2.1 *Materials*

Bismuth(III) nitrate pentahydrate, sodium molybdate dehydrate, ethylene glycol, ethanol, isopropanol, sodium bromide, silver nitrate, MB, RhB, phenol, p-benzoquinone, ammonium oxalate and other routine chemicals were analytical grade and used without further purification. Deionized water was used throughout all experiments.

2.2 *Preparation of Ag/AgBr/Bi_2MoO_6 composite*

Bi_2MoO_6 was prepared through a simple alcohol-thermal procedure. Typically, 3.37 g of $Bi(NO_3)_3{\cdot}5H_2O$ and 1.84 g of $Na_2MoO_4{\cdot}2H_2O$ were dissolved separately in 10 ml of ethylene glycol under magnetic stirring. The two solutions were mixed, and then 40 ml of ethanol was added slowly into the mixed solution with stirring for another 10 min. The resulting clear solution was transferred into a 100 ml Teflon-lined stainless steel autoclave. The sealed autoclave was heated to 160°C, kept at the temperature for 24 h, and then cooled down to room temperature. The obtained sample was filtered, washed with ethanol, dried at 60°C for 6 h, and calcined at 400°C for 2 h.

Ag/AgBr/Bi_2MoO_6 was synthesized by deposition precipitation together with photoreduction. Typically, 0.31 g of the obtained solid was added into 50 ml of 0.012 mol l^{-1} NaBr solution and ultrasonicated for 30 min. Then, 6.25 ml of 0.10 mol l^{-1} $AgNO_3$ solution was slowly dropped with continuous stirring for 3 h in a dark. Afterwards, the suspension was irradiated using a 300 W xenon lamp with stirring for 10 min. The achieved precipitate was centrifuged and washed with absolute ethanol 3 times, and then dried at 60°C for 6 h. The obtained sample was named Ag/AgBr/Bi_2MoO_6. For comparison, Ag/AgBr was prepared without the addition of Bi_2MoO_6; AgBr/Bi_2MoO_6 and Ag/Bi_2MoO_6 were prepared based on the procedure described above.

2.3 *Catalysts characterization*

The phase structure of the obtained products was measured on a powder X-ray diffraction (XRD, Bruker D8 Advance diffractometer) with Cu-K_α radiation (Kα = 1.5406 Å) in the range of 2θ = 10°–70°. The surface morphology was carried out on a field-emission scanning electron microscopy (FESEM, Nova NanoSEM 450) equipped with an energy X-ray dispersive spectrometer (EDS). The X-ray photoelectron spectroscopy (XPS) analysis was performed on a Thermo Scientific ESCALAB 250Xi X-ray photoelectron spectrometer using Al Kα X-ray as the excitation source. The C 1s peak at 284.8 eV of the surface adventitious carbon was used as the reference. Shimadzu UV-2450 spectrophotometer was used to perform UV-vis diffuse reflectance spectra (DRS) in the wavelength range of 200–800 nm with $BaSO_4$ as background. Shimadzu RF-5301PC fluorescent spectrophotometer was used to measure room temperature photoluminescence (PL) spectra with an excitation wavelength of 320 nm.

2.4 *Photocatalytic activity*

The obtained photocatalysts were used to evaluate their photocatalytic activities through the degradation of RhB, MB and phenol under visible-light irradiation. The visible light came from a 300 W Xe lamp filtered with a 420 nm ultraviolet cutoff. A constant height of 15 cm was kept between the lamp and reactor. For the degradation of RhB (100 ml, 5 mg l^{-1}), MB (100 ml, 5 mg l^{-1}) and phenol (100 ml, 10 mg l^{-1}), 50 mg of photocatalyst was added into the aqueous solution. An adsorption–desorption equilibrium was acquired between photocatalyst and dye molecules prior to irradiation and thus was magnetically stirred for 30 min in the dark. During the irradiated procedure, 4 ml of suspension was taken out by a syringe at intervals and centrifuged to remove the photocatalyst. The concentration of RhB was analysed on a PerkinElmer Lamda 35 UV–vis spectrophotometer.

To analyse the active species of the Ag/AgCl/Bi_2MoO_6, isopropanol (IPA), *p*-benzoquinone (BQ) and ammonium oxalate (AO) were added into mixed RhB solution including the catalyst and were used to capture hydroxyl radicals (•OH), superoxide radicals ($\bullet O_2^-$) and holes (h^+), respectively. Then, the photocatalytic test was performed under visible-light irradiation and a UV-vis spectrophotometer was used to measure the residual RhB concentration.

3. Results and discussion

3.1 *XRD analysis*

The structure and composition of the as-obtained samples were characterized by XRD, as shown in figure 1. Figure 1a exhibits characteristic diffraction peaks at 2θ values of about 23.4, 28.2, 32.4, 35.9, 46.7, 47.1, 55.4, 56.1, 58.4 and 68.1, corresponding to the (111), (131), (200), (151), (202), (060), (331), (191), (262) and (400) crystal planes of orthorhombic Bi_2MoO_6 (JCPDS No. 76-2388), respectively. Figure 1e shows four diffraction peaks of 26.7°, 31.1°, 44.4°, 55.1° and 64.6°, matching well with the corresponding (111), (200), (220), (222) and (400) crystal planes of cubic AgBr (JCPDF No. 79-0149). The appeared diffraction peaks of AgBr in figure 1c and d reveal the formation of well-crystallized AgBr NPs on Bi_2MoO_6 through Ag^+ and Br^- deposition.

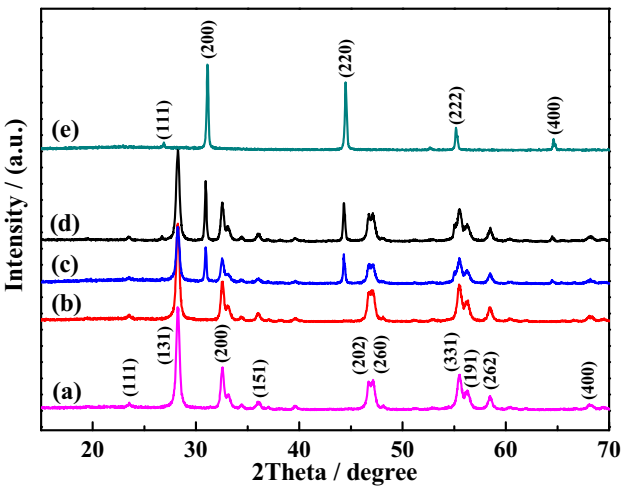

Figure 1. XRD patterns of (**a**) Bi_2MoO_6, (**b**) Ag/Bi_2MoO_6, (**c**) AgBr/Bi_2MoO_6, (**d**) Ag/AgBr/Bi_2MoO_6 and (**e**) Ag/AgBr.

In addition, the colour of the suspension Ag/AgBr, Ag/Bi_2MoO_6 and Ag/AgBr/Bi_2MoO_6 changed from light yellow to greyish with increased photoreduction time during the preparation. It indicates the existence of Ag^0, which is attributed to the transformation of AgBr under UV–visible irradiation. However, no diffraction peak assigned to Ag^0 appears in the XRD pattern of all samples, demonstrating the very fine Ag^0, which could not be detected by the current XRD technique due to its low content. The result proves that the production of Ag^0 can be attributed to the pyrolysis of AgBr. Furthermore, compared to pure Bi_2MoO_6, the Bi_2MoO_6 diffraction peaks in Ag/Bi_2MoO_6 and Ag/AgBr/Bi_2MoO_6 do not have any shift, which suggests that Ag and AgBr are only deposited on the Bi_2MoO_6 surface. Therefore, it is clear that this method can successfully construct the Ag/AgBr/Bi_2MoO_6 composite.

3.2 *SEM and EDS analysis*

Figure 2 shows the morphologies of Bi_2MoO_6 and Ag/AgBr/Bi_2MoO_6 by FESEM images. The pure Bi_2MoO_6 exhibits hierarchical floriated hollow spheres composed of a large number of smooth nanoplates, confirming its typical Aurivillius phase with layered structure (figure 2a and b). The nanoplates terminated with $[Bi_2O_2]^{2+}$ layers are in favour of the absorption of Br^- by electrostatic interaction [7]. Thus, AgBr NPs are formed on the surface of Bi_2MoO_6 through deposition by the sequencing addition of KBr and $AgNO_3$. Then, hierarchical Ag/AgBr/Bi_2MoO_6 composite is achieved by the photoreduction of partial AgBr under UV–visible light irradiation. Therefore, the Ag/AgBr/Bi_2MoO_6 composite maintains a constant morphology with Bi_2MoO_6 confirmed by FESEM images (figure 1c and d).

Additionally, the elemental distribution of hierarchical Ag/AgBr/Bi_2MoO_6 composite was analysed by energy dispersive X-ray spectrometry (EDS). Figure 3 shows elemental maps for a selected FESEM image. As seen, the elements of Bi, Mo, Ag, Br and O are uniformly distributed and retain the image morphology of Ag/AgBr/Bi_2MoO_6, confirming that Ag/AgBr particles are highly dispersed on the Bi_2MoO_6 surface.

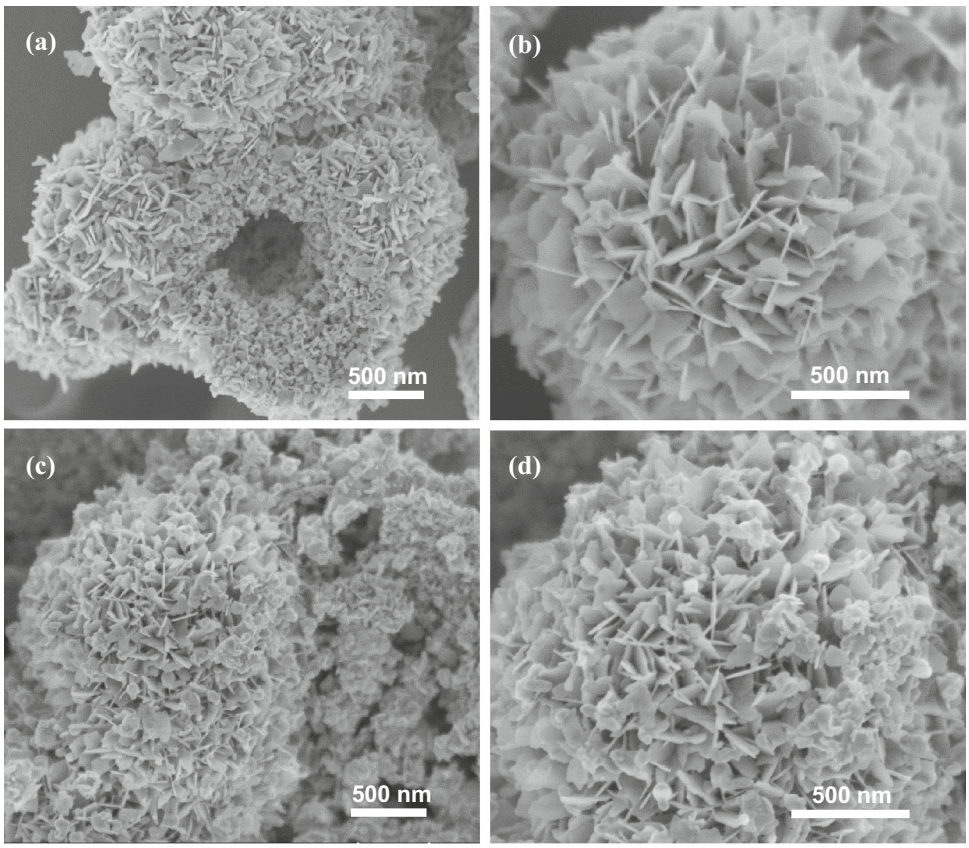

Figure 2. FESEM images of (**a**, **b**) Bi_2MoO_6 and (**c**, **d**) $Ag/AgBr/Bi_2MoO_6$.

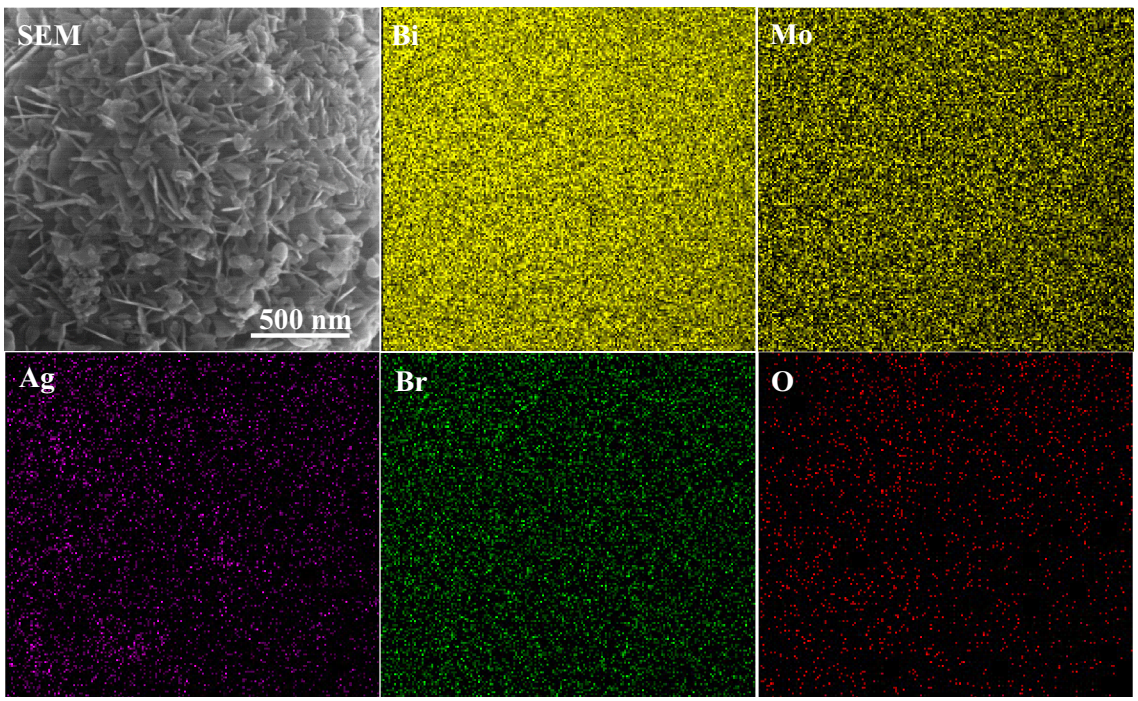

Figure 3. EDS elemental mapping images of $Ag/AgBr/Bi_2MoO_6$.

3.3 *XPS analysis*

The chemical composition and surface structure of the prepared Ag/AgBr/Bi_2MoO_6 composite were further measured by XPS and the results are shown in figure 4. Figure 4a shows the survey XPS spectrum of Ag/AgBr/Bi_2MoO_6, which is composed of Ag, Br, O, Mo and Bi elements originated from the Ag, AgBr and Bi_2MoO_6 components without any unlabelled element. Figure 4b shows two peaks at approximately 159.6 and 164.9 eV responding to the binding energies of Bi $4f_{7/2}$ and Bi $4f_{5/2}$ of Bi^{3+}, respectively [26]. For the Mo profile (figure 4c), the peaks at 232.8 and 236.0 eV reference to the binding energies of Mo $3d_{5/2}$ and Mo $3d_{3/2}$ [26]. The O 1s spectrum can break up into three different peaks, in figure 4d, demonstrating the presence of different O species in Ag/AgBr/Bi_2MoO_6 composite. Two dominant peaks contribute to lattice oxygen in Bi_2MoO_6 with Bi-O and Mo-O, corresponding to binding energies of 530.3 and 530.9 eV, respectively [26]. The other peak corresponds to

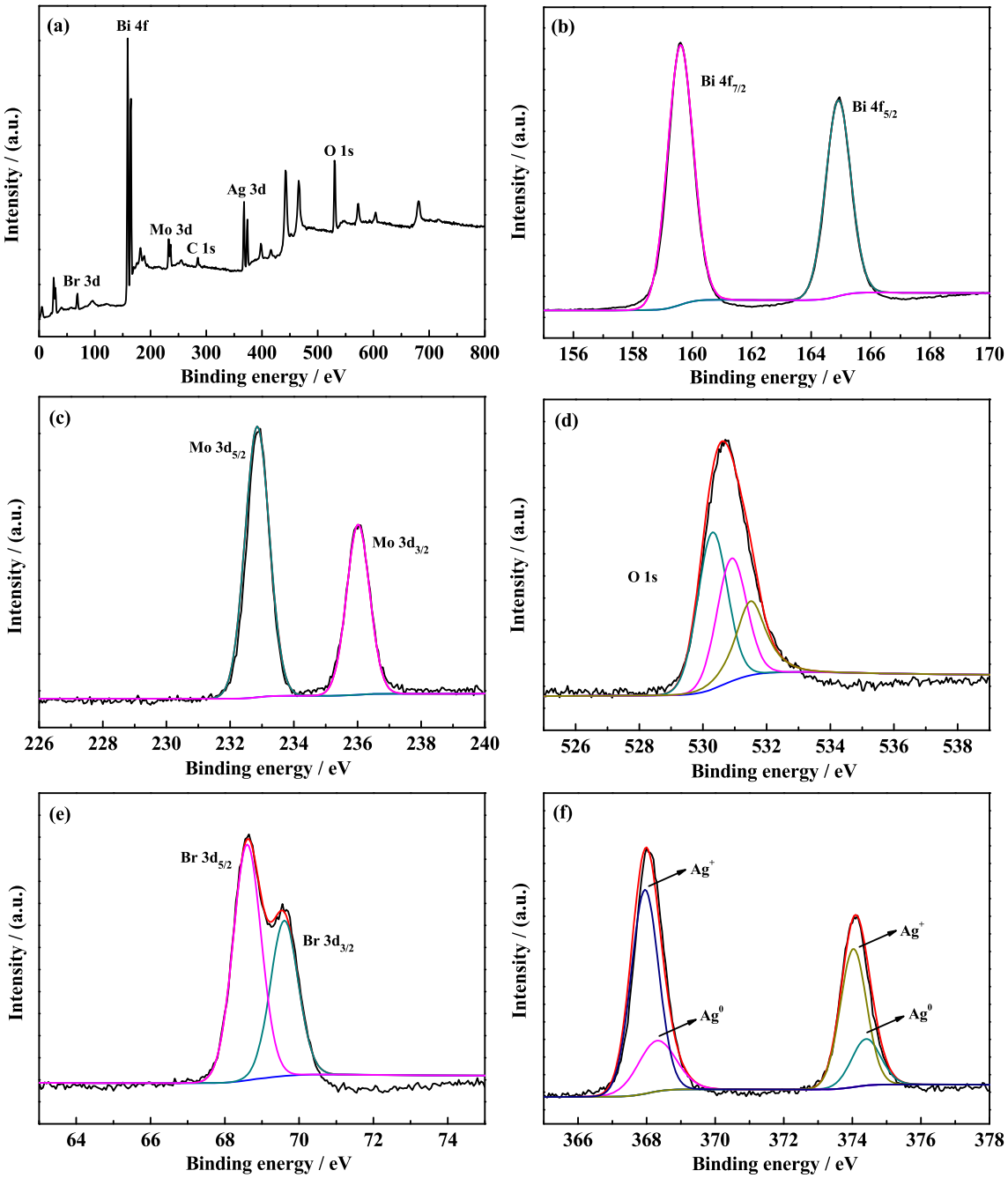

Figure 4. (**a**) The XPS full spectrum of Ag/AgBr/Bi_2MoO_6, high-resolution XPS spectra for (**b**) Bi 4f, (**c**) Mo 3d, (**d**) O 1s, (**e**) Br 3d and (**f**) Ag of Ag/AgBr/Bi_2MoO_6.

chemisorbed oxygen of surface hydroxyl (–OH) at a relatively high binding energy of 531.5 eV [7].

Figure 4e shows the XPS spectrum of Br $3d_{5/2}$ and Br $3d_{3/2}$ with binding energies at 68.6 and 69.6 eV, assigning to Br^- state of AgBr [27]. The high-resolution Ag 3d spectrum in figure 4f can be divided into two sets of symmetric peaks. The strong peaks at approximately 367.9 and 374.0 eV are attributed to the binding energies of Ag $3d_{5/2}$ and Ag $3d_{3/2}$ of Ag^+ in AgBr, respectively [28]. The weak peaks with the binding energies at 367.8 and 373.8 eV are assigned to Ag $3d_{5/2}$ and Ag $3d_{3/2}$ of Ag^0 due to the photoreduction of partial AgBr [28]. According to the above results of XPS and EDS analysis, they confirm the presence of Ag, AgBr and Bi_2MoO_6 in the prepared composite.

3.4 *Photocatalytic activity and kinetics*

The photocatalytic activities of Ag/AgBr/Bi_2MoO_6 composite and compared catalysts were evaluated by the degradation of RhB, MB and phenol under visible-light irradiation. Figure 5a shows the degradation curves of RhB over Bi_2MoO_6, Ag/AgBr/Bi_2MoO_6, AgBr/Bi_2MoO_6, Ag/Bi_2MoO_6 and Ag/AgBr. In the absence of catalyst (blank), the degradation of RhB solution is negligible, which indicates that the self-photolysis of RhB can be ignored. Bi_2MoO_6 shows very weak activity, and can only degrade 13% of RhB within 15 min irradiation. Ag/Bi_2MoO_6, Ag/AgBr, AgBr/Bi_2MoO_6 and Ag/AgBr/Bi_2MoO_6 composites exhibit much higher photocatalytic activities than the sole Bi_2MoO_6 under the same conditions, and the degradation efficiencies are 21, 72, 90 and 95%, respectively. The Ag/AgBr/Bi_2MoO_6 film could degrade 97% of MB in 60 min and the Ag/AgBr/Bi_2MoO_6 prepared under SDA exhibited degradation efficiency (98%) of MB within 120 min [24,25]. Therefore, the Ag/AgBr/Bi_2MoO_6 prepared without the addition of SDA is more efficient for the degradation of MB than the reported Ag/AgBr/Bi_2MoO_6. Notably, about 23 ± 1% of RhB has been adsorbed for AgBr/Bi_2MoO_6 and Ag/AgBr/Bi_2MoO_6 photocatalysts in the dark with an adsorption–desorption equilibrium. The electrostatic interaction between anionic MoO_4^{2-} layers and the cationic $=N^+(CH_2CH_3)_2$ group of RhB dye is responsible for the high adsorption capacity, because of Ag/AgBr and Ag/AgCl NPs dispersed on the $(Bi_2O_2)^{2+}$ layers [29]. Based on the above results, it can be deduced that the synergistic effect of the components in the Ag/AgBr/Bi_2MoO_6 system could be crucial for its excellent photocatalytic activity.

Additionally, either *N*-dealkylation or direct cleavage of the conjugated chromophore structure would occur for the visible light-irradiated photocatalytic degradation of *N*-alkyl-containing dyes [30]. The degradation procedures

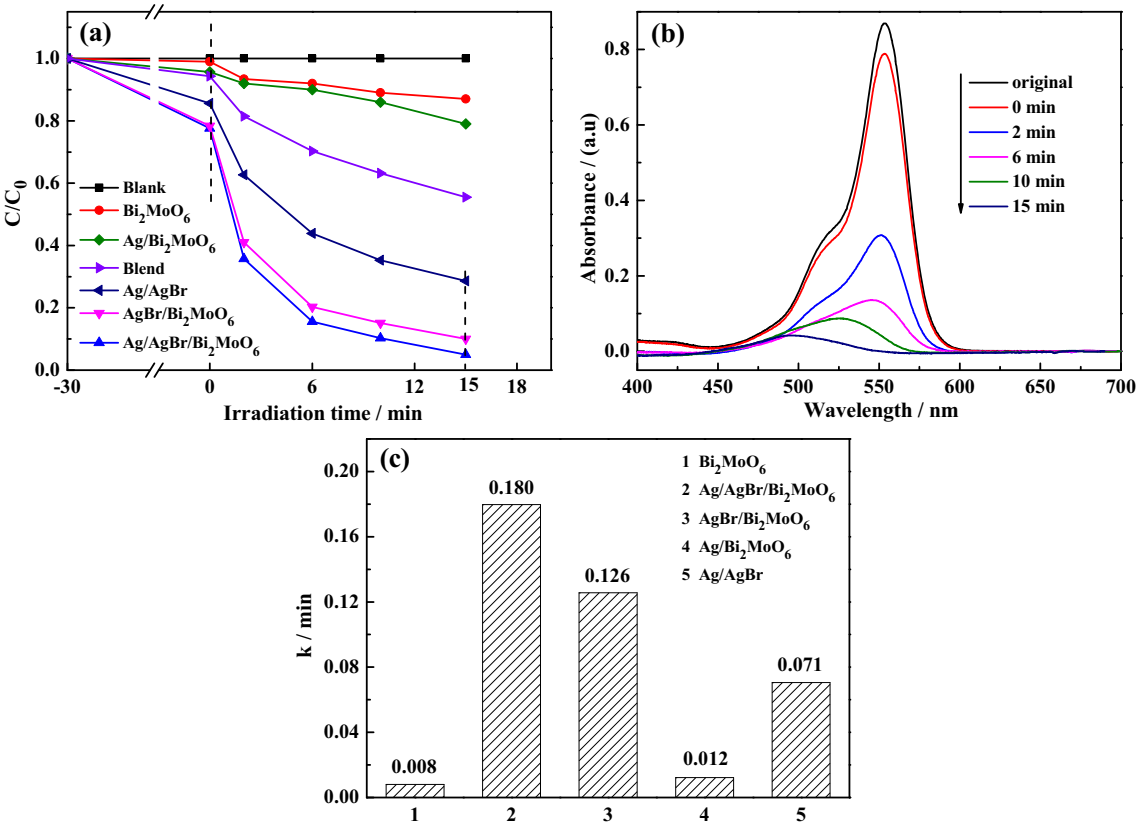

Figure 5. (**a**) Photocatalytic activities of different photocatalysts, (**b**) visible light absorbance spectra of Ag/AgBr/Bi_2MoO_6 and (**c**) apparent reaction rate constants of different photocatalysts for RhB degradation.

of RhB dye depend on the adsorption modes, carboxylic (–COOH) group and cationic $=N^{+}(CH_2CH_3)_2$ group on the surface of the photocatalysts. Generally, RhB dye molecules result in direct cleavage of the RhB chromophore structure with the carboxylic adsorption, while forming *N*-deethylated intermediates with cationic $=N^{+}(CH_2CH_3)_2$ adsorption under visible irradiation. For the Ag/AgBr/Bi_2MoO_6 composite, the maximum absorbance peak of RhB gradually decreases and exhibits an evident blue shift from 554 to 498 nm (figure 5b), ascribing to form *N*-deethylated intermediates in the photocatalytic degradation [29,30]. Therefore, the adsorption of the dye occurred via the $=N^{+}(CH_2CH_3)_2$ group is well in agreement with the high adsorption capacity of the Ag/AgBr/Bi_2MoO_6 described above, which shows the *N*-deethylation process in the Ag/AgBr/Bi_2MoO_6 system.

To quantify the removing efficiency of the photocatalytic reaction process, the apparent reaction rate constant of RhB photocatalytic degradation was obtained based on the typical Langmuir-Hinshelwood first-order reaction kinetics. As shown in figure 5c, for the degradation of RhB, the apparent reaction rate constants are calculated to be 0.008, 0.180, 0.126, 0.012 and 0.071 min^{-1} for Bi_2MoO_6, Ag/AgBr/Bi_2MoO_6, AgBr/Bi_2MoO_6, Ag/Bi_2MoO_6 and Ag/AgBr, respectively. It demonstrates Ag/AgBr/Bi_2MoO_6 presents the highest rate constant, which is approximately 2.5 times than that of Ag/AgBr and 22.5 times as high as Bi_2MoO_6. These results show the Ag/AgBr/Bi_2MoO_6 composite can efficiently degrade RhB under visible-light illumination. The superior photoreactivity of Ag/AgBr/Bi_2MoO_6 can be ascribed to the strong synergetic effects of Ag/AgBr and Bi_2MoO_6.

Furthermore, the photocatalytic degradation of MB and colourless phenol under visible-light illumination was also utilized to evaluate the photocatalytic performance of the Ag/AgBr/Bi_2MoO_6. As shown in figure 6a, the Ag/AgBr/Bi_2MoO_6 composite shows the best photocatalytic performance and can decompose 90% of MB within only 15 min. The photocatalytic performances of the compared catalysts for the MB degradation under the same conditions are also shown and the photoreactivity order of these catalysts is highly consistent with the above results for RhB degradation. Additionally, to rule out the photosensitization effect under visible-light irradiation, the hierarchical Ag/AgBr/Bi_2MoO_6 composite was also used to photodegrade a non-dye organically chemical, phenol. The photodegradation efficiency in figure 6b clearly shows its high photocatalytic efficiency in comparison with other catalysts. Therefore, the hierarchical Ag/AgBr/Bi_2MoO_6 composite can exhibit improved photocatalytic activities for the degradation of RhB, MB and phenol.

Besides the excellent photocatalytic activity, the recyclability of the photocatalyst is important for practical application. The recycle experiments for RhB degradation over the Ag/AgBr/Bi_2MoO_6 composite were measured under visible-light illumination. As shown in figure 7, the Ag/AgBr/Bi_2MoO_6 composite can completely decompose RhB within 15 min in the initial two cycles and has a slight loss after the second cycling run. Then it remains a stable photocatalytic performance and achieves 90% of RhB photodegradation efficiency after the fourth cycle. The slight loss of photocatalytic activity could be mainly attributed to the reduction of AgBr during the twice cycles or produced intermediates covered on the surface of photocatalyst particles.

The reused Ag/AgBr/Bi_2MoO_6 was collected and performed by XRD and SEM after the fourth cycle. As shown in figure 8a, the XRD patterns show no significant difference for the Bi_2MoO_6 diffraction peaks before and after the fourth cycle of photodegradation experiments. It is also important to note that the diffraction intensity of AgBr decreased slightly. A weak diffraction peak at 38.1° appears assigned to (111) reflection of Ag (JCPDS 87-717), which is in good agreement with the expected AgBr reduction during the initial twice reaction cycles. The SEM image (figure 8b) also demonstrates that the photocatalytic oxidation process

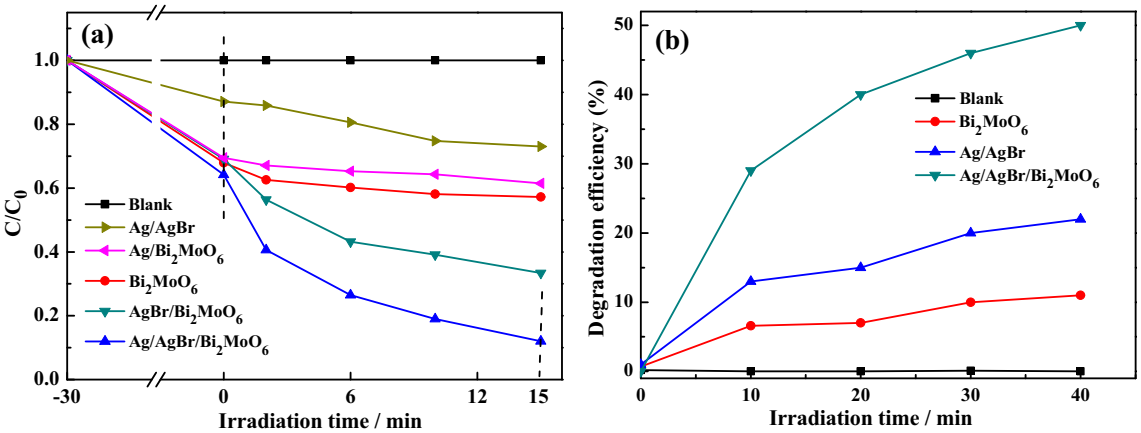

Figure 6. (**a**) Photocatalytic activities for MB degradation and (**b**) removing efficiencies of phenol over different photocatalysts.

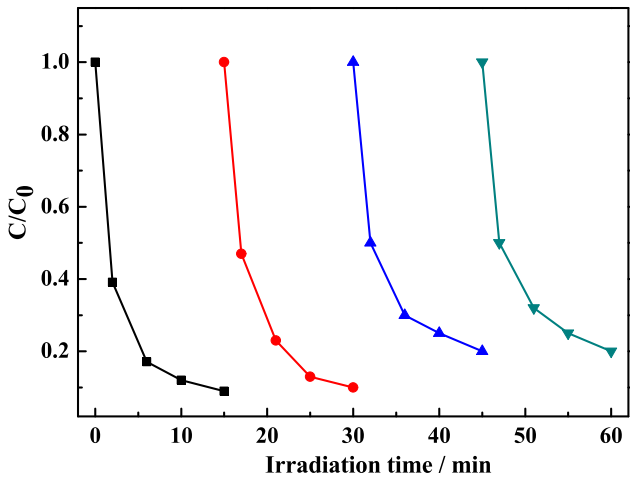

Figure 7. Recyclability for degradation RhB of Ag/AgBr/Bi_2MoO_6 under visible-light irradiation.

does have any influence on the morphology of the catalyst. These results indicate that the hierarchical Ag/AgBr/Bi_2MoO_6 composite has outstanding photostability under visible-light illumination.

3.5 *UV–vis diffuse reflectance analysis*

The photocatalytic performance of a photocatalyst is somehow related to its optical absorption property. UV–vis diffuse reflectance spectra were used to investigate the absorption capability of Ag/Bi_2MoO_6, Ag/AgBr, Ag/AgBr/Bi_2MoO_6, AgBr/Bi_2MoO_6 and Bi_2MoO_6, as shown in figure 9a. The sole Bi_2MoO_6 has a weak visible light response with a terminated absorption band edge of about 490 nm. The optical bandgap energy of the Bi_2MoO_6 was estimated by Mulliken electronegativity theory and the X-intercept of the tangent line gives an approximation of the bandgap energy of the Bi_2MoO_6 (figure 9b) [31]. Thus, the optical bandgap energy of Bi_2MoO_6 is 2.80 eV, which matches well with the reported 2.74 eV [32].

It can be seen that the loading of AgBr onto the surface of Bi_2MoO_6 leads to an enhanced absorption ability in the visible-light region due to the fact AgBr can also be responsive to visible light with the appropriate bandgap of 2.82 eV [33]. For Ag/Bi_2MoO_6, Ag/AgBr and Ag/AgBr/Bi_2MoO_6, there is a wide absorption shoulder band at 400–700 nm attributing to the localized SPR of Ag NPs [34]. Binary Ag/Bi_2MoO_6 and Ag/AgBr composites show high visible absorption ability, however, their photoactivities are lower than Ag/AgBr/Bi_2MoO_6. The fact is that excessive Ag NPs result in a fast electron–hole recombination rate with low photoactivity [35]. These results indicate that the ternary Ag/AgBr/Bi_2MoO_6 composite has a different photocatalytic mechanism from those of binary composites, which leads to superior visible-light photocatalytic activity. Therefore, besides SPR role, Ag NPs may dominantly act as the Z-scheme bridge in the Ag/AgBr/Bi_2MoO_6 system, which also has been proved in Ag/AgBr/Bi_2WO_6 [5], Ag/AgBr/BiOBr [17] and all-solid-state Z-scheme photocatalytic systems [1].

3.6 *PL analysis*

In addition, room temperature PL is a powerful tool to analyse the recombination rate of the photogenerated electron–hole pairs, which has an important influence on photocatalytic activity. The recombination of electron–hole pairs can release energy corresponding to the fluorescence emission [36,37]. In general, the weaker PL intensity means the lower electron–hole recombination rate and the higher photocatalytic activity. As shown in figure 10, Bi_2MoO_6-based photocatalysts exhibit similar emission peaks located about 420–580 nm, and Ag/AgBr/Bi_2MoO_6 exhibits the

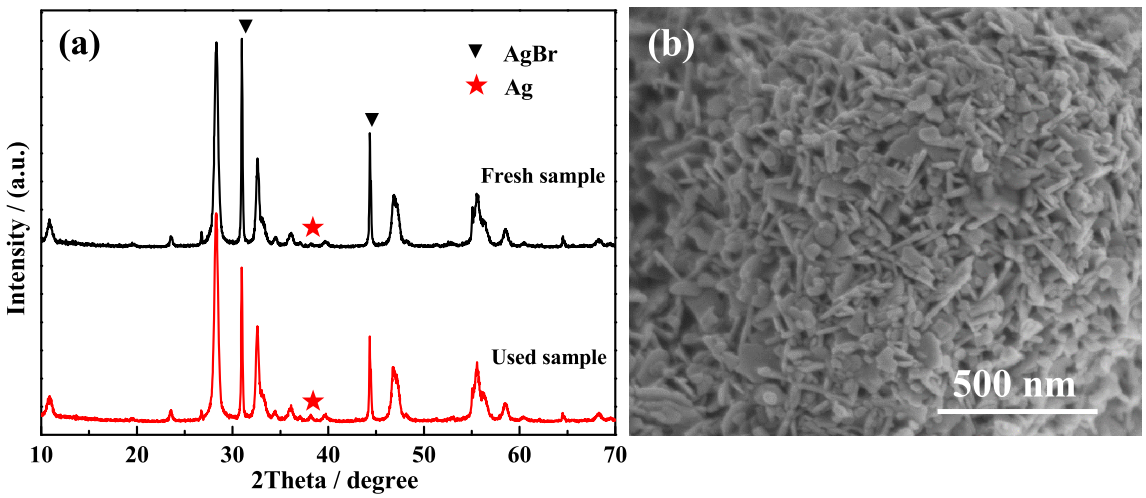

Figure 8. (**a**) XRD patterns, (**b**) FESEM image of the used Ag/AgBr/Bi_2MoO_6 after the degradation of RhB under visible-light irradiation.

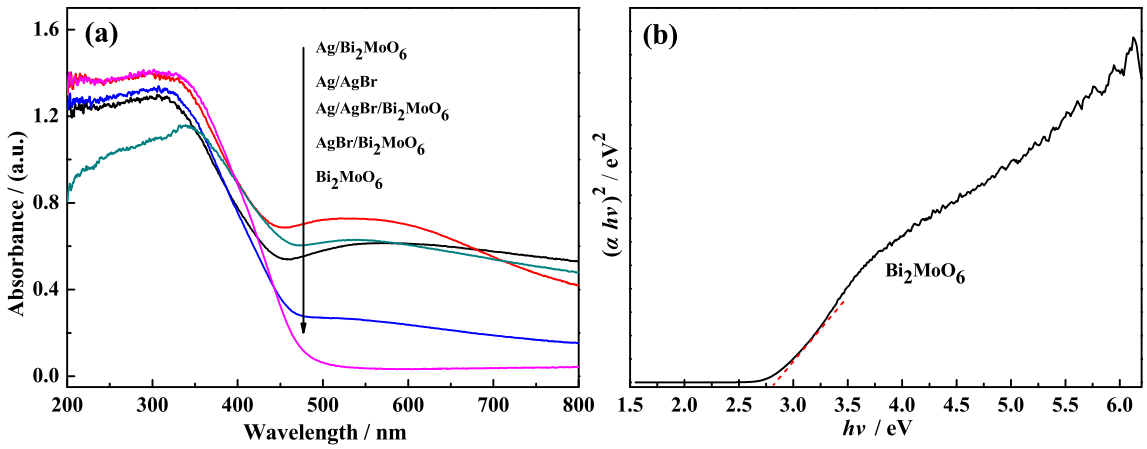

Figure 9. (**a**) UV–vis diffuse reflectance spectra of different photocatalysts and (**b**) the bandgap determination of Bi_2MoO_6.

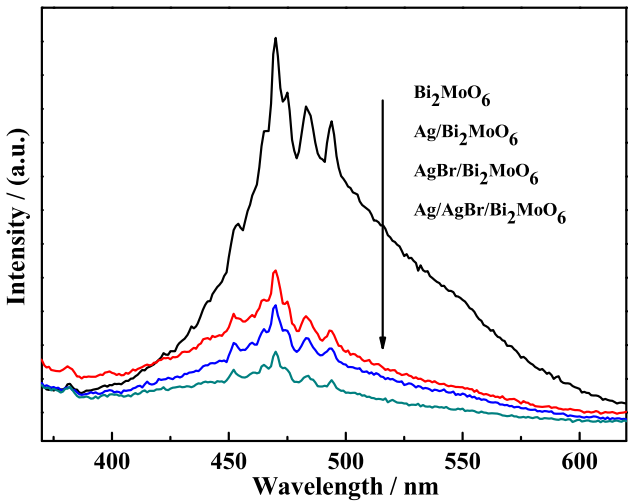

Figure 10. Room-temperature PL spectra of different photocatalysts.

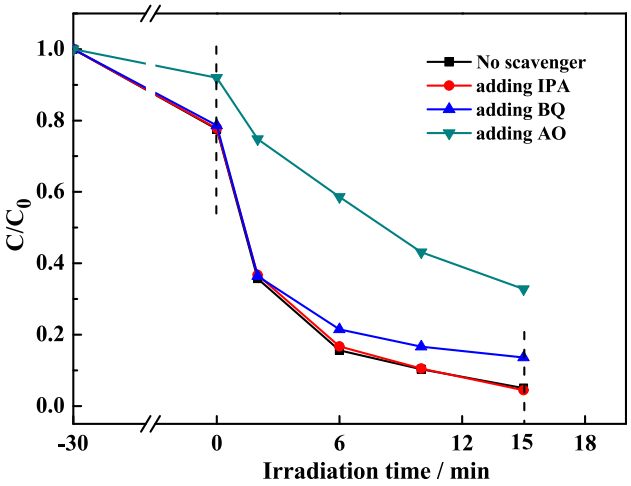

Figure 11. Reactive species trapping experiments over Ag/$AgBr/Bi_2MoO_6$ catalyst under visible-light irradiation.

lowest emission intensity. The weakest emission intensity in the $Ag/AgBr/Bi_2MoO_6$ demonstrates the lowest recombination of electron–hole pairs, which indicates the best photodegradation activity. The results are in good accordance with the aforementioned photocatalytic results.

3.7 *Photocatalytic mechanism analysis*

For the $Ag/AgBr/Bi_2MoO_6$ composite, to investigate the visible photocatalytic mechanism, the main active species were explored by the free radical trapping experiments. In the experiments, IPA, BQ and AO as the scavengers of hydroxyl radicals (•OH), superoxide radicals ($\bullet O_2^-$) and photoinduced holes (h^+) were introduced into the photoreaction, respectively. Figure 11 shows the photocatalytic efficiency of RhB photodegradation over the Ag/AgBr/Bi_2MoO_6 in the presence of different scavengers. The addition of IPA into the RhB solution does not have any influence on the photocatalytic activity, which indicates •OH plays a negligible role during the photocatalytic process. The photocatalytic activities are inhibited after the addition of AO and BQ into the dye solution, which illustrates that h^+ and $\bullet O_2^-$ act as the dominant active species. Therefore, the dye molecules are mainly attacked by h^+ and $\bullet O_2^-$ during the photocatalytic reaction of Ag/AgBr/Bi_2MoO_6.

Thus, the Z-scheme photocatalytic mechanism for feasible charge separation process over the hierarchical Ag/$AgBr/Bi_2MoO_6$ composite under visible-light illumination is proposed in figure 12. The Ag NPs *in-situ* generated at the contact interface between conductors Bi_2MoO_6 and AgBr forms a low-resistance Ohmic contact, which reduces the distance of Z-scheme electron transfer [38,39]. Herein, both Bi_2MoO_6 and AgBr can be excited under visible-light irradiation owing to their suitable bandgap energy of 2.80 and 2.82 eV [32], respectively. The electrons and holes are separately photogenerated (steps 1 and 2) in their conductor

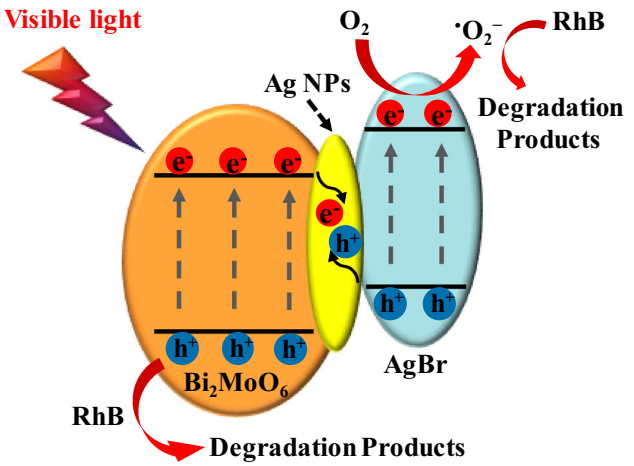

Figure 12. Photocatalytic reaction mechanism under visible-light irradiation.

band (CB) and valence band (VB). The electrons in the CB of Bi_2MoO_6 (BMO_{CB}) easily flow into metal Ag through the Schottky barrier, since the CB potential of Bi_2MoO_6 is more negative than that Fermi level of the loaded Ag NPs (step 3). On the contrary, the Fermi level of Ag is more positive than the VB of AgBr ($AgBr_{VB}$), so the holes in the VB of AgBr also easily flow into Ag NPs (step 4), which is faster than the electron–hole recombination between the VB and CB of AgBr.

Therefore, electron transfers enhance the separation of both holes in the VB of Bi_2MoO_6 and electrons in the CB of AgBr. The holes can directly mineralize dye molecules due to their strong oxidation abilities (step 5). Simultaneously, the electrons can react with oxygen molecules in water to generate a superoxide radical anion, which also degrades the adsorbed dye molecules (steps 6 and 7). As a result, the Ag/AgBr/Bi_2MoO_6 composite shows improved photocatalytic activity. The detailed Z-scheme photocatalytic degradation processes are as follows:

$$Bi_2MoO_6 + \text{visible light} \rightarrow e^- + h^+ \quad (1)$$

$$AgBr + \text{visible light} \rightarrow e^- + h^+ \quad (2)$$

$$BMO_{CB} + e^- \rightarrow Ag + e^- \quad (3)$$

$$AgBr_{VB} + h^+ \rightarrow Ag + h^+ \quad (4)$$

$$h^+ + \text{dye} \rightarrow \text{degraded products} \quad (5)$$

$$e^- + O_2 \rightarrow \bullet O_2^- \quad (6)$$

$$\bullet O_2^- + \text{dye} \rightarrow \text{degraded products} \quad (7)$$

4. Conclusion

The hierarchical Ag/AgBr/Bi_2MoO_6 composite was prepared through hydrothermal and subsequent precipitation-photoreduction methods. The synthesized Ag/AgBr/Bi_2MoO_6 composite showed higher photocatalytic activity than binary Ag/AgBr, AgBr/Bi_2MoO_6, Ag/Bi_2MoO_6 and pristine Bi_2MoO_6 for the degradation of RhB, MB and phenol under visible-light irradiation. Moreover, it remained high stability after the fourth cycle of photocatalytic reaction of RhB. The enhanced photocatalytic performance can be mainly ascribed to the Z-scheme photocatalytic degradation processes, in which Ag NPs dominantly act as the Z-scheme bridge for electron transfer, and thus improve the separation of electron–hole pairs. Therefore, the Z-scheme Ag/AgBr/Bi_2MoO_6 composite with improved visible-light photoactivity has potential for practical application in wastewater purification.

Acknowledgements

The work was financially supported by Natural Science Foundation of Shanghai (No. 19ZR1412500) and the National Natural Science Foundation of China (No. 21776074, 21861132019).

References

[1] Peydayesh M, Suter M K, Bolisetty S, Boulos S, Handschin S, Nyström L *et al* 2020 *Adv. Mater.* **32** 1907932
[2] Yu C, Zhou W, Hong L, Yuan L and Dionysiou D D 2016 *Chem. Eng. J.* **287** 117
[3] Dil M A, Haghighatzadeh A and Mazinani B 2019 *Bull. Mater. Sci.* **42** 248
[4] Hemamalini S and Manimekalai R 2021 *Bull. Mater. Sci.* **44** 154
[5] Miao G, Chen L and Qi Z 2012 *Eur. J. Inorg. Chem.* **2012** 5864
[6] Jada N, Sankaran K J, Sakthivel R, Sethi D and Mohapatra P 2021 *Bull. Mater. Sci.* **44** 167
[7] Zhu Q, Wang Z, Chen L, Cheng H and Qi Z 2018 *ACS Appl. Nano. Mater.* **1** 5083
[8] Cui Y M, Li H Q, Hong W S, Fan S H and Zhu L J 2013 *Powder Technol.* **247** 151
[9] Fan H M, Wang D J, Wang L L, Li H Y, Wang P, Jiang T F *et al* 2011 *Appl. Surf. Sci.* **257** 7758
[10] Zhang J, Niu C G, Ke J, Zhou L F and Zeng G M 2015 *Catal. Commun.* **59** 30
[11] Liu X T, Gu S N, Zhao Y J, Zhou G W and Li W J 2020 *J. Mater. Sci. Technol.* **56** 45
[12] Stelo F, Kublik N, Ullah S and Wender H 2020 *J. Alloys Compd.* **829** 154591
[13] Wang T Y, Zhang F J, Xiao G S, Zhong S and Lu C 2015 *Photochem. Photobiol.* **91** 291
[14] Chen Y J, Tian G H, Shi Y H, Xiao Y T and Fu H G 2015 *Appl. Catal. B Environ.* **164** 40
[15] Zhang J L, Zhang L S, Yu N, Xu K B, Li S J, Wang H L *et al* 2015 *RSC Adv.* **5** 75081
[16] An Y, Cao W, Zhou Y, Chen L and Qi Z 2017 *Appl. Organomet. Chem.* **31** 3777
[17] Ye L Q, Liu J Y, Gong C Q, Tian L H, Peng T Y and Zan L 2012 *ACS Catal.* **2** 1677

[18] Li Y F, Zhao Y, Fang L, Jin R X, Yang Y and Xing Y 2014 *Mater. Lett.* **126** 5
[19] Zou X J, Dong Y Y, Li S J, Ke J and Cui Y B 2018 *Sol. Energy* **169** 392
[20] Yu J J, Sun D P, Wang T H and Li F 2018 *Chem. Eng. J.* **334** 225
[21] Ding K, Yu D, Wang W, Gao P and Liu B J 2018 *Appl. Surf. Sci.* **445** 39
[22] Xu Y G, Liu Q Q, Liu C C, Zhai Y P, Xie M, Huang L Y *et al* 2018 *J. Colloid Interf. Sci.* **512** 555
[23] Yang L, Ye F Y, Liu P and Wang F Z 2016 *Photochem. Photobio.* **92** 800
[24] Yang R X, Zhao Q Q and Liu B J 2020 *J. Mater. Sci. Mater. Electron.* **31** 5054
[25] Liu Y J, Zhou F, Zhan S and Yang Y F 2017 *J. Inorg. Organomet. Polym.* **27** 1365
[26] Wang D J, Shen H D, Guo L, Fu F and Liang Y C 2016 *New J. Chem.* **40** 8614
[27] Jonjana S, Phuruangrat A, Thongtem T and Thongtem S 2016 *Mater. Lett.* **172** 11
[28] He J, Shao D W, Zheng L C, Zheng L J, Feng D Q, Xu J P *et al* 2017 *Appl. Catal. B: Environ.* **203** 917
[29] Yao C H, Wang X J, Zhao W, Li T F, He Y L, Ran X *et al* 2020 *J. Alloys Compd.* **846** 156335
[30] Wang Q, Chen C C, Zhao D, Ma W H and Zhao J C 2008 *Langmuir* **24** 7338
[31] Cao W, Chen L and Qi Z 2014 *Catal. Lett.* **144** 598
[32] Kashfi-Sadabad R, Yazdani S, Alemi A, Huan T D, Ramprasad R and Pettes M T 2016 *Langmuir* **32** 10967
[33] Dai K, Li D P, Lu L H, Liu Q, Liang C H, Lv J L *et al* 2014 *Appl. Surf. Sci.* **314** 864
[34] Wang X F, Li S F, Ma Y Q, Yu H G and Yu J G 2011 *J. Phys. Chem. C* **115** 14648
[35] Ge L, Han C C, Liu J and Li Y F 2011 *Appl. Catal. A: Gen.* **409** 215
[36] Cao W, Gui Z, Chen L, Zhu X and Qi Z 2017 *Appl. Catal. B: Environ.* **200** 681
[37] Cao W, Chen L and Qi Z 2015 *J. Mol. Catal. A: Chem.* **401** 81
[38] Chen F, Yang Q, Li X M, Zeng G M, Wang D B, Niu C G *et al* 2016 *Appl. Catal. B: Environ.* **200** 330
[39] Ren M L, Chen J, Wang P F, Hou J, Qian J, Wang C *et al* 2018 *J. Colloid Interf. Sci.* **532** 190